

STUDY OF TYPICAL WATER HEADER FLOW STRUCTURE BY LARGE EDDY SIMULATION AND RANS

by

Hao QIN^a, Bin WANG^b, Yun GUO^a, and Miao HU^{c*}

^a School of Nuclear Science and Technology,
University of Science and Technology of China, Hefei, China
^b China Ship Development and Design Center, Wuhan, China

^c Department of Chemical and Materials Engineering, Hefei University, Hefei, China

Original scientific paper
<https://doi.org/10.2298/TSCI210607293Q>

Water header is the most common structure in the design of flow system for energy and power system. The complex flow structure could result in some problems when CFD simulation is applied in the whole system analysis. The rapid change in velocity distribution of the flow field leads to difficulties to create suitable boundary-layer mesh, and the complex flow structure will also make residuals hard to reach convergence criteria. Large eddy simulation is promising to promote these studies, it is more accurate than RANS method and can capture many non-steady-state characteristics those RANS method cannot obtain. In this study a typical water header flow structure is investigated by RANS and large eddy simulation methods. By comparing the detailed flow structures in the results of two methods, the deficiency of RANS method was found. The results of large eddy simulation can be used to guide the establishment of meshes and the application of time-averaged turbulence models to improve efficiency in engineering. The asymmetric Reynolds stresses may induce asymmetric flow field in symmetric geometry.

Key words: water header; large eddy simulation, RANS

Introduction

The RANS method is widely used in engineering design, because it can provide acceptable results with less computing resource. However, RANS has its limits, it cannot accurately predict secondary flow and higher-order statistics in complex structures and some special structures, such as sudden expansion, sudden contraction, disturbing device, *etc.* Water header is a typical structure in flow system, which looks like a combination of expansion and contraction. The boundary-layer will separate and reattach. The flow will hit the opposite wall. The adjacent pipes can affect each other. Hence, the geometry of water header is not very complex, but it contains many difficulties in numerical simulation such as flow separation, turbulent mixing, and vortex generation [1]. The water header is responsible for the flow convergence and flow distribution, sometimes we need to reduce or simplify the calculation of other calculation domain to ensure that the water header calculation is accurate because of limited computing resources [2]. In transient case the flow from the pipes into the header and the flow from the header into the pipes will often induce vortices and complex secondary flow [3, 4], which need appropriate turbulence model to do the analysis. In addition, the flow dissipation and head loss

* Corresponding author, e-mail: miaohu1979@163.com

related to viscosity coefficient will be produced in the process of sudden expansion [5]. The $k-\varepsilon$ turbulence model is proved to be feasible. The absolute pressure data of intake manifold under three engine speeds and three throttle openings were obtained by Galambos *et al.* [6], which are consistent with the experimental data. Su *et al.* [7] also used the $k-\varepsilon$ model to simulate the sudden expansion process of the jet impingement chamber. The results show that there is a strong transverse flow structure.

Water header is often part of a whole flow system, hence, an appropriate turbulence model is not only benefit for itself but also good for the whole flow system, such as reducing the amount of calculation and improving the accuracy of calculation. Although each RANS model declares its advantage in some kind flow or structure it is still very hard to select one appropriate model for water header because of so many special difficulties as aforementioned. However, sometimes one better RANS model (if there is one) must be selected for design or development in engineering. So, these RANS models can be evaluated with large eddy simulation (LES) in advance. Here we did not choose experimental data as validation or chosen criterion. The applicability and generalization of CFD or the RANS model are not good enough. A RANS model chosen based on one experiment is not very convincing. Therefore, present paper aims to evaluate the RANS models from the viewpoint of flow field by LES. Or in other words, if all the RANS models have no significant differences in the simulation, then simpler model with small calculation quantity will be preferred in engineering.

In present paper, four typical RANS models were utilized to study the flow characteristics of the water header. At the same time LES was also performed to study the flow characteristics of the same structure. The RANS models are discussed based on the results of LES. The two objectives of the study are:

- providing detailed flow field and turbulent statistics in a typical simplified header in support of validating RANS models and
- enhancing the understanding of flow phenomena in a typical simplified water header and providing reference for the thermal-hydraulic design of flow system.

Numerical and computational details

Governing equations

Turbulent flows are characterized by eddies with a wide range of length and time scales. The large eddies which are typically comparable in size to the characteristic length of the mean flow, are directly resolved by LES. The small eddies those are responsible for the dissipation of turbulence kinetic energy, are assumed to be isotropic and universal, and are modeled statistically by subgrid model.

In LES, the variables are divided into a filtered (grid-scale) part and a residual (sub-grid-scale) part using a filtering function. For velocity $u_i = \bar{u}_i + u'$, the filtered governing equations of LES for incompressible turbulent flow are expressed [8]:

$$\frac{\partial \bar{u}_i}{\partial x_i} = 0 \quad (1)$$

$$\frac{\partial \bar{u}_i}{\partial t} + \frac{\partial (\bar{u}_i \bar{u}_j)}{\partial x_j} = -\frac{1}{\rho} \frac{\partial \bar{p}}{\partial x_i} - \frac{\partial \tau_{ij}}{\partial x_j} + \frac{\partial}{\partial x_j} \left[\nu \frac{\partial \bar{u}_i}{\partial x_j} \right] \quad (2)$$

$$\tau_{ij} = \overline{u_i u_j} - \bar{u}_i \bar{u}_j \quad (3)$$

where \bar{u}_i and \bar{p} are filtered velocity and pressure, respectively, τ_{ij} – the subgrid scale shear stress resulting from the filtering operation. The Boussinesq hypothesis is employed to compute τ_{ij} from:

$$\tau_{ij} - \frac{1}{3}\tau_{kk}\delta_{ij} = -2\mu_t\bar{S}_{ij} \quad (4)$$

where δ_{ij} is the Kronecker delta, μ_t – the eddy viscosity to be modeled, and \bar{S}_{ij} is the rate-of-strain tensor defined:

$$\bar{S}_{ij} = \frac{1}{2}\left[\frac{\partial\bar{u}_i}{\partial x_j} + \frac{\partial\bar{u}_j}{\partial x_i}\right] \quad (5)$$

The WALE subgrid scale model [9] is employed to model eddy viscosity. This model is recommended to study wall-bounded flows, and it returns a zero turbulent viscosity for laminar shear flows, which allows the correct treatment of laminar zones. The eddy viscosity μ_t is computed:

$$\mu_t = \rho(C_w\Delta)^2 \frac{(S_{ij}^d S_{ij}^d)^{3/2}}{(\bar{S}_{ij}\bar{S}_{ij})^{5/2} + (S_{ij}^d S_{ij}^d)^{5/4}} \quad (6)$$

where $C_w = 0.325$ is the model constant, Δ and S_{ij}^d are defined:

$$\Delta = C_w V^{1/3} \quad (7)$$

$$S_{ij}^d = \frac{1}{2}\left(\frac{\partial\bar{u}_i}{\partial x_k} \frac{\partial\bar{u}_k}{\partial x_j} + \frac{\partial\bar{u}_j}{\partial x_k} \frac{\partial\bar{u}_k}{\partial x_i}\right) - \frac{1}{3}\delta_{ij} \frac{\partial\bar{u}_k}{\partial x_l} \frac{\partial\bar{u}_l}{\partial x_k} \quad (8)$$

The details of RANS models, such as $k-\epsilon$ model, $k-\omega$ model, SST model and RSM model can be found in [10].

Computational domain and boundary conditions

The computational geometry is a simplified header as shown in fig. 1. The diameter of the inlet pipe is 10 mm, and so is the hydraulic diameter, D_{hy} . The inlet is at $-10D_{hy}$, and the outlet is at $10D_{hy}$. The total length of the geometry is 200 mm which corresponds to $20D_{hy}$. The length of the header is 50 mm, and the area of the cross-section is $60 \times 60 \text{ mm}^2$. Meanwhile, a fully developed turbulent flow with a constant mass-flow rate was employed in the two inlets. The fully developed inlet condition was computed from a sufficient long pipe and transferred to the two inlets. The outlet used a standard condition based on an imposed pressure and zero Neumann boundary conditions for the other variables. The boundary condition for the wall was set as no-slip boundary. Water flows into the two inlets with a nominal velocity, W , of 0.5 m/s, leading to a Reynolds number of about 4991 based on the hydraulic diameter. The density and dynamic viscosity of water are 998.2 kg/m^3 and $1 \cdot 10^{-3} \text{ Pa}\cdot\text{s}$, respectively. It should be noted that the purpose of this study is to understand the flow behavior in a simplified typical header using LES with affordable computing resources.

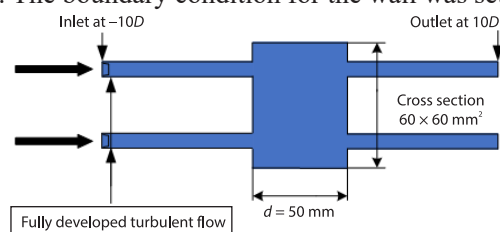


Figure 1. Computational domain and boundary conditions

The main computational domain and boundary conditions of RANS models are the same as those of LES. The inlet is fully developed flow, which is obtained by extending the length of two inlet pipes.

Mesh study

In RANS simulations, the mesh has to be refined until the solutions are independent from grid number. However, in LES study, the mesh needs to be refined to achieve the resolution requirement. If the resolution requirement is achieved, the results will approach the direct numerical simulation results. According to Choi and Moin [11], $\Delta x^+ \approx 15\sim 30$, $N_y \approx 15\sim 30$, and $\Delta z^+ \approx 50\sim 130$ are recommended as grid resolution requirement, in which Δx^+ and Δz^+ are the spanwise and streamwise resolutions, respectively, and N_y is the node number normal to the wall. Figure 2 displays the overall view of mesh of the simplified header. The spanwise and streamwise resolutions of the mesh are $\Delta x^+ = 15.6$ and $\Delta z^+ = 58.5$, respectively, which satisfy the requirement for wall resolved LES. In the direction normal to the wall, the height of the first mesh in the wall adjacent cell is 0.04 mm. Figure 3 shows the distribution of wall y^+ , it can be seen that most of the wall cells reaches the requirement that y^+ is less than 1. Although a few cells on the wall close to the outlet are slightly higher, 99% of the wall cells satisfy the requirement. In the boundary-layer region, $N_y = 20$ is placed. In the streamwise region the grid number is set to 165, which leads the cell length in the inlet and outlet pipe of 1.5 mm and the header region cell length of 0.2 mm. Total grid number is about 2 million in the computational domain.

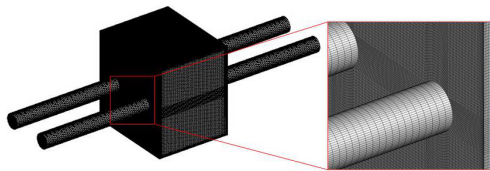


Figure 2. View of the structural mesh

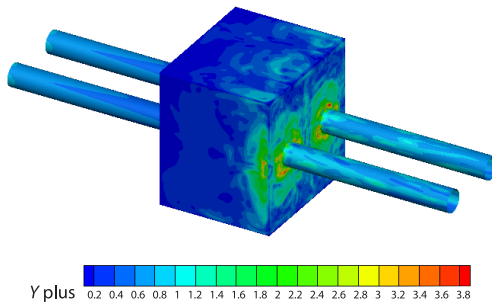


Figure 3. Distribution of wall y^+

For comparison, the same mesh is used in RANS too. So in $k-\epsilon$ model the enhanced wall function can be used. And the mesh is also fine enough for RSM model.

Numerical set-up

The numerical simulation was performed using CFD package FLUENT 18.0. The second order bounded-central difference scheme was utilized to discretize convection term. This scheme has been verified to have good accuracy and robustness, and is recommended by the FLUENT manual as the scheme for LES of complex flows. The second-order implicit scheme was applied to discretize the unsteady term. According to the Courant-Friedrichs-Lewy condition, Courant number should be below 0.5, so the time step was set to $\Delta t = 1 \cdot 10^{-4}$ seconds to ensure this criterion. The residuals were set to $1 \cdot 10^{-5}$, and the inner iteration within each time step was set to 100. At each time step, the solution could converge within 26 iterations. The simulation was first run for 2 seconds (five flow through time) to get a statistical stable turbulent flow, and then run for another 4 seconds (ten flow through time) for collecting average statistics. Figure 4 shows the measured cross-section and measured line. The instantaneous velocity and pressure were collected at central line, Points A and B. The data were recorded every time step. The numerical case was run on a cluster of 64 cores and 128 GB memory in the supercomputing center of USTC. The total wall-clock time was about three weeks.

For RANS models this is a stable calculation. It only takes 6-20 hours for RANS models to reach the same convergence criterion $1 \cdot 10^{-5}$ on a workstation with 32 cores and 128 GB memory.

Results and discussion

Time-averaged flow properties

The streamwise velocity field, which affects the heat transfer characteristics and flow distribution, is of great interest in the thermal-hydraulic design of power system. Figure 5 displays instantaneous streamwise velocity contour of the central plane of the computational domain. The instantaneous streamwise velocity field is obtained by LES simulation, and large eddies and anisotropic turbulent structures were captured in transient simulation. This is one of the main advantages that LES is preferable compared to RANS. Figure 6 illustrates the streamlines of the mean velocity magnitude contour at central plane, there four large eddies near the wall, which can be interpreted as fluid hitting the wall and then flowing back. These large eddies related to boundary conditions can both be captured in LES and RANS simulations, fig. 7, while the small eddies and anisotropic turbulent structures can only be captured in LES simulation.

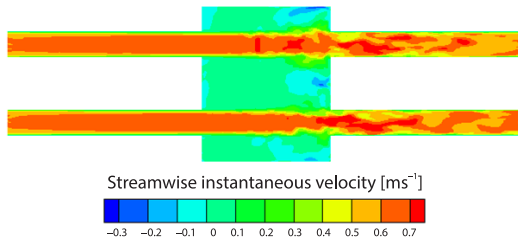


Figure 5. Distribution of the instantaneous streamwise velocity

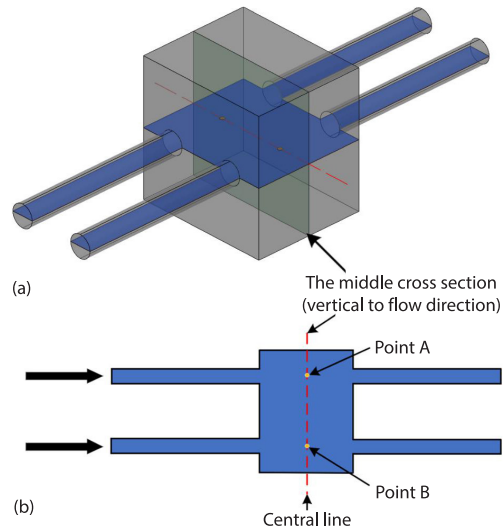


Figure 4. Data-collected regions; (a) at the middle cross-section of the channel and (b) at the central line of the middle cross-section

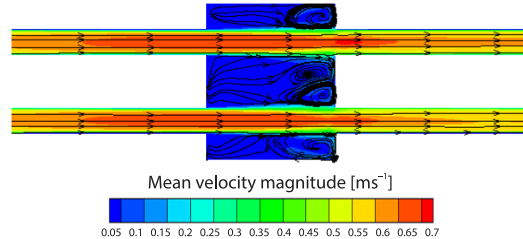


Figure 6. Streamlines of the mean velocity magnitude

Figure 7 shows the time-averaged streamwise mean velocity contours obtained from LES and RANS simulation at the central plane. It is observed that $k-\epsilon$ model and RSM show similar distribution of streamwise mean velocity fields. When the fluid-flows into the header, the velocity of the mainstream gradually decreases until the fluid-flows out the header. In the results of $k-\omega$ model and SST model, the maximum streamwise velocity is a little smaller and the mainstream velocity does not decrease significantly. This phenomenon is significantly different from the other three models. The streamwise velocity in the header looks very uniform in the results of $k-\omega$ model and SST model. The $k-\epsilon$ model and RSM predict lower streamwise velocity in the header. In the LES results, the mainstream flow field is similar as $k-\epsilon$ model and RSM model, but in the water header LES predicts lower streamwise velocity, which is different from all the RANS models. The LES captures stronger reverse flow.

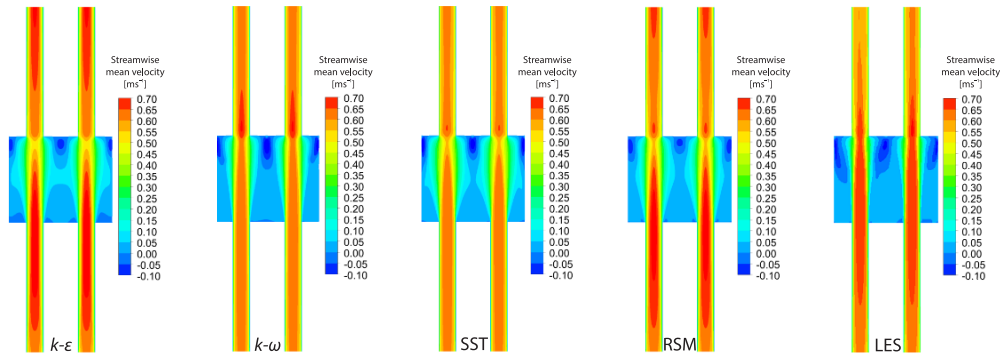


Figure 7. Distributions of the time-averaged mean streamwise velocity of different models

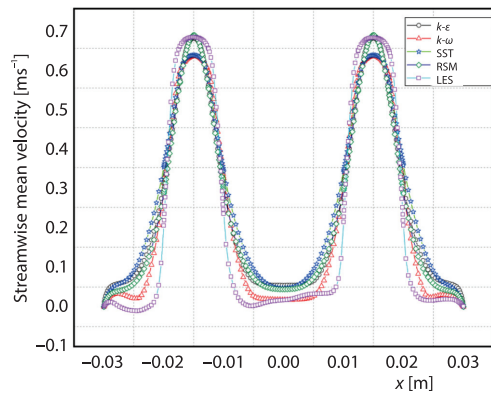


Figure 8. The time-averaged mean streamwise velocity at measuring line

other line are chosen different results will be obtained. As we know, comparing the velocity distribution along one line is often used in the CFD analysis. In this case the defect is obvious, which cannot reflect the advantages and disadvantages in the results of whole flow field. Hence, in complex geometry the main flow field is the key point of comparison, instead of line or point.

As a whole, both RANS and LES can capture the large eddies connected to geometry boundary, but the flow details in the velocity contour are different. From the point of view for main flow field the $k-\varepsilon$ model and RSM model are better. The $k-\varepsilon$ model has more advantages if computation quantity is considered. It should be noticed that in the result of LES the flow field is not symmetrical although the geometry is symmetric. At the same time all the results of RANS models are symmetric. Because of the chaotic nature of turbulent pulsations and the unpredictable variation of vortices in the transient the flow field cannot be symmetric. Hence, RANS's idea of forced averaging leads to these symmetrical results.

Cross-sectional secondary flow

Secondary flow is brought about by the anisotropic turbulent stresses (*i.e.* Reynolds normal and shear stresses) on the cross-section of the flow channel. The secondary flow intensity that determines fluid mixing and heat transfer coefficient is one critical property and should be carefully investigated in engineering design. The middle cross-section selected is shown in fig. 4. Figure 9 illustrates the turbulent intensity of four different RANS models in the selected

If these results are looked at in another way maybe some different points of view can be found. The streamwise mean velocities at the measuring line, fig. 4, were plotted in fig. 8. The distribution law is similar in RANS models and LES. At this line LES predicts significantly lower velocity in the header, and the main-stream velocity distribution is flatter and more like fully developed turbulent velocity distribution. From the view of velocity distribution, the results of $k-\omega$ model and SST model are more similar as LES, but $k-\omega$ model and SST model predict lower velocity in the peak, while $k-\varepsilon$ model and RSM model predict more accurately. Obviously, if the velocity distributions of another

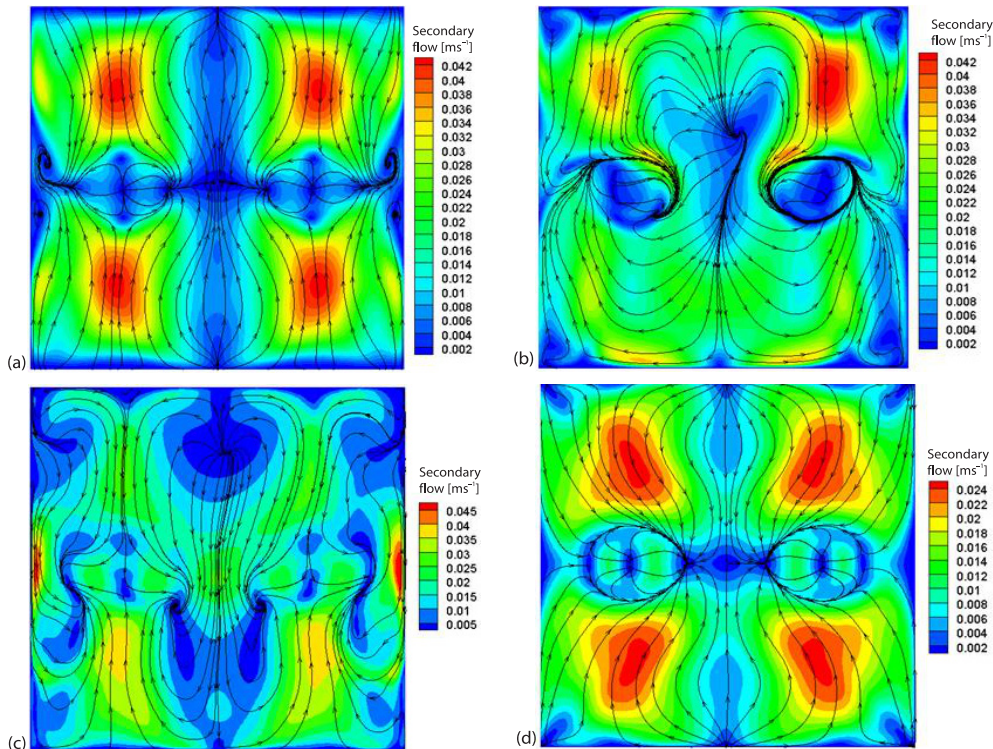


Figure 9. Distributions of the secondary flow by RANS; (a) $k-\epsilon$, (b) $k-\omega$, (c) SST, and (d) RANS

middle cross-section (vertical to flow direction). In the simulation results of $k-\epsilon$ model, it is observed that, the location where secondary flow intensity is higher, symmetrically distributes in the middle parts of four quadrants, and the secondary flow intensity reaches 0.042 m/s. The location of lower secondary flow intensity is distributed in the cross area, and there are some small eddies captured in the area adjacent to wall. The streamlines show that the fluid-flows into the center in the secondary flow field, which will increase the mixing and enhance heat transfer in the header. In the simulation results of $k-\omega$ model, the overall secondary flow intensity distribution is similar but asymmetric. The low secondary flow intensity in the mainstream area is observed. The secondary flow intensity reaches 0.042 m/s, which is the same as that of $k-\epsilon$ model. The SST model is four equations model. It should be more accurate than $k-\epsilon$ model and $k-\omega$ model which are two equations model. In the simulation results of SST model, it is observed that the secondary flow intensity is a little higher, and the mainstream region shows higher secondary flow intensity. The secondary flow intensity reaches 0.045 m/s, the location where secondary flow intensity is highest is adjacent to wall, which is unique among the four models. The RSM model that is a six equations model should be the most accurate RANS model at present. The overall distribution of secondary flow intensity is similar as the result of $k-\epsilon$ model except the value of secondary flow. The maximum secondary flow intensity that RSM predicts reaches 0.024 m/s, and the value is lowest among four models. Hence, the results of four RANS model differ significantly. Only the distributions of secondary flow intensity in RSM model and $k-\epsilon$ model are similar. Therefore, it is very difficult to evaluate these RANS models based on the results of secondary flow.

Figure 10 illustrates the instantaneous secondary flow and mean secondary flow in the selected middle cross-section obtained in LES simulation. In the instantaneous secondary flow field, the maximum secondary flow intensity reaches 0.18 m/s in the region where main-stream flows past, and there are lots small eddies captured. In the mean secondary flow field, the maximum secondary flow intensity reaches 0.09 m/s in the similar location, and there are some small eddies near the wall. These small eddies promote mixing and local disturbance, and thus enhance the heat transfer behaviors. In comparing with the results of RANS models, LES results predict the overall secondary flow stronger.

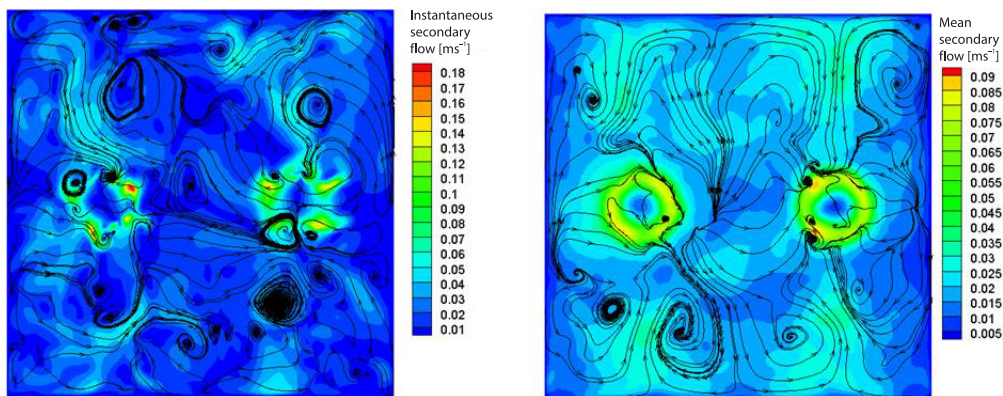


Figure 10. Distributions of the secondary flow by LES

Hence, from the point of secondary flow all the RANS models are not good enough compared with LES in distribution and value. Normally, it is very difficult for RANS models to accurately predict the secondary flow field and capture the small eddies near the wall. The RANS models cannot reflect the transient characteristics of flow field, which can be obtained by LES study. Therefore, it is difficult to select an appropriate RANS model based on secondary flow.

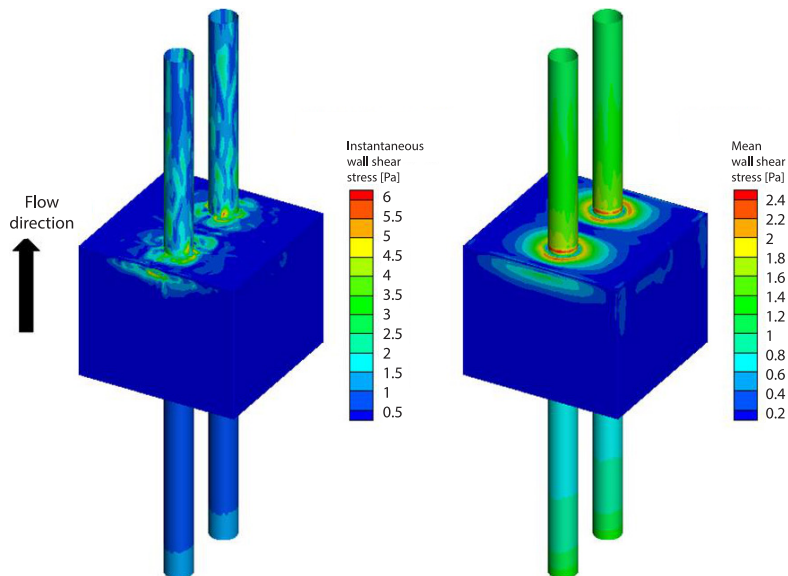


Figure 11. Distributions of the wall shear stress on the wall by LES

Here it can be summarized that at least for present geometry only the comparison of main flow field is meaningful. The comparisons of values at special lines or points and secondary flow field are not valid.

Wall shear stress and second-order statistics

The RANS model has natural defects for complex structures and flows. The random pulsation of turbulence will induce time varying wall shear stress as displayed in fig. 11 obtained in LES results.

The wall shear stress around the wall close to the outlet is higher and reaches 2.4 Pa, while the wall shear stress in side walls of the header is below 0.2 Pa. This is attributed to strong secondary flow and the motion of large eddies in the region close to the outlet. In the instantaneous wall shear stress distribution, it is also observed in the wall of outlet pipe that the turbulent stripes have been reproduced, which further demonstrates an adequate resolution of presented LES.

The time averaged mean Reynolds stresses obtained in RSM and LES on the measuring line are exhibited in fig. 12. The Reynolds stresses are also caused by random pulsation of turbulence, which should be carefully investigated in CFD simulations. At the wall of the water header all the Reynolds stresses reduce to 0, because non-slip condition is applied to the wall. For $\overline{U'W'}$ component, the RSM predicts two peaks (one positive and one negative) in the region where mainstream flows past, the distribution is centrosymmetric for the left and right sides. The LES results show similar distributions but predict lower $\overline{U'W'}$ Reynolds stresses. For $\overline{V'W'}$ and $\overline{W'W'}$ Reynolds stresses, RSM model obtained equally 0 value almost, while LES

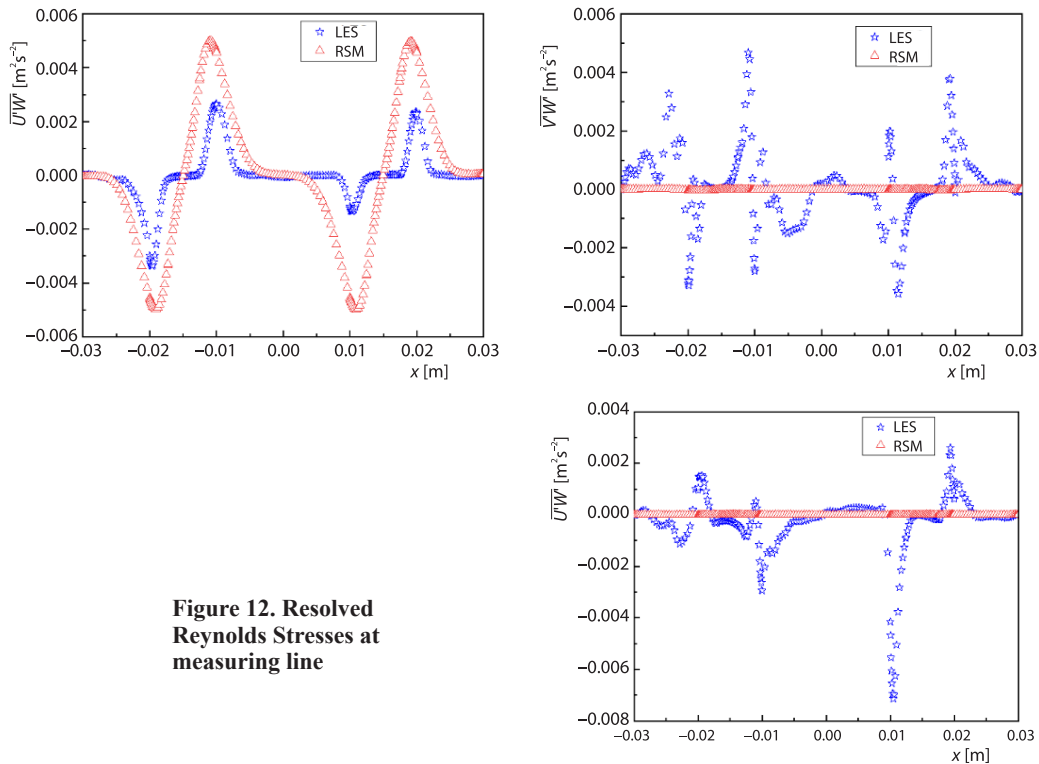


Figure 12. Resolved Reynolds Stresses at measuring line

obtained larger values those are an order of magnitude smaller than $\bar{U}'W'$ Reynolds stress. The RSM model that is a time-averaged model can not obtain transient properties of the turbulence, while LES model can capture the transient properties of the anisotropic turbulent flow. In transient calculations, LES can predict $\bar{U}'W'$, $\bar{V}'W'$ and $\bar{W}'W'$ Reynolds stresses more accurately, and that is what RANS method can not achieve. Furthermore, the Reynolds Stresses are not symmetrical, which may be the reason for asymmetric flow field in symmetrical geometry.

Conclusions

The turbulent flow in a typical water header has been studied using RANS and LES. Based on the numerical results, the conclusions can be drawn as follows.

- Using inlet profile to give a fully developed turbulent velocity distribution can significantly reduce the computational resources, and thus allows for LES simulation at acceptable computational time and resources.
- Based on the detailed comparison, it is very difficult to select one appropriate RANS model. In engineering, it is recommended to only consider the mainstream flow field and the model with less computation quantity.
- The asymmetric Reynolds stresses induce asymmetric flow field in symmetric geometry. RANS idea of forced averaging leads to symmetrical results.
- The LES can find more detailed information of flow field and permits therefore, a good understanding of much flow phenomenon. It can be used in the evaluation of RANS, especially for some special structures such as: orifice, grid spacer, and triple valve. The LES is obviously more objective than just comparing the results of RANS.

References

- [1] Naeimi, H., *et al.*, A Parametric Design of Compact Exhaust Manifold Junction in Heavy Duty Diesel Engine Using Computational Fluid Dynamics Codes, *Thermal Science*, 15 (2011), 4, pp. 1023-1033
- [2] Fan, W. Y., *et al.*, An optimized CFD Method for Conceptual Flow Design of Water Cooled Ceramic Blanket, *International Journal of Hydrogen Energy*, 42 (2017), 31, pp. 20138-20145
- [3] Li, X., *et al.*, The inlet Flow Blockage Accidents Analysis in the Rectangular Flow Channel of Water Cooled Blanket, *Fusion Engineering and Design*, 171 (2021), 112605
- [4] Fan, W. Y., *et al.*, A New CFD Modelling Method for Flow Blockage Accident Investigations, *Fusion Engineering and Design*, 303 (2016), July, pp. 31-41
- [5] Zhang, H. C., *et al.*, Flow and Heat Transfer Characteristics of Nanofluids in Sudden Expansion Structure Based on Sla Method, *Thermal Science*, 23 (2019), 3, pp. 1449-1455
- [6] Galambos, S. L., *et al.*, An Approach to Computational Fluid Dynamic Air-Flow Simulation in the Internal Combustion Engine Intake Manifold, *Thermal Science*, 24 (2020), 1, pp. 127-136
- [7] Su, Z. G., *et al.*, Study on Diesel Cylinder-Head Cooling Using Nanofluid Coolant with Jet Impingement, *Thermal Science*, 19 (2015), 6, pp. 2025-2037
- [8] Pope, S. B., *Turbulent Flows*, Cambridge University Press, Cambridge, UK, 2000
- [9] Nicoud, F., Ducros, F., Subgrid-Scale Stress Modelling Based on the Square of the Velocity Gradient Tensor, *Flow Turbul and Combust*, 62 (1999), 3, pp. 183-200
- [10] ***, Fluent Inc., FLUENT 18.0. user's guide, USA, 2016
- [11] Choi, H., Moin, P., Grid-Point Requirements for Large Eddy Simulation: Chapman's Estimates Revisited, *Physics of Fluids*, 24 (2012), 1, 011702